Loading Bose-Einstein-condensed atoms into the ground state of an optical lattice

P. S. Julienne,[1] C. J. Williams,[1] Y. B. Band,[2] and Marek Trippenbach[3]
[1]*Atomic Physics Division, 100 Bureau Drive Stop 8423, National Institute of Standards and Technology, Gaithersburg, Maryland 20899–8423, USA*
[2]*Departments of Chemistry, Electro-Optics, and The Ilse Katz Center for Nano Science, Ben-Gurion University of the Negev, Beer-Sheva 84105, Israel*
[3]*Institute for Theoretical Physics, Optics Division, Warsaw University, ul. Hoża 69, Warsaw 00-681, Poland*
(Received 22 December 2004; published 16 November 2005)

We optimize the turning on of a one-dimensional optical potential, $V_L(x,t)=S(t)V_0\cos^2(kx)$ to obtain the optimal turn-on function $S(t)$ so as to load a Bose-Einstein condensate into the ground state of the optical lattice of depth V_0. Specifically, we minimize interband excitations at the end of the turn-on of the optical potential at the final ramp time t_r, where $S(t_r)=1$, given that $S(0)=0$. Detailed numerical calculations confirm that a simple unit cell model is an excellent approximation when the turn-on time t_r is long compared with the inverse of the band excitation frequency and short in comparison with nonlinear time $\hbar/\mu$ where μ is the chemical potential of the condensate. We demonstrate using the Gross-Pitaevskii equation with an optimal turn-on function $S(t)$ that the ground state of the optical lattice can be loaded with no significant excitation even for times t_r on the order of the inverse band excitation frequency.

DOI: 10.1103/PhysRevA.72.053615 PACS number(s): 03.75.Lm, 67.90.+z, 32.80.Qk

I. INTRODUCTION

A number of competing schemes for implementing quantum information and quantum computing are being explored; five physical systems have been proposed as quantum logic gates, ion traps [1], high-Q optical cavities [2,3], nuclear magnetic resonance systems [4], solid-state qubits (semiconductor quantum-dot and Josephson-junction devices) [5,6], and ultracold neutral atoms in optical lattices [7,8]. The proposals for using atoms in optical lattices can be implemented by first loading Bose condensed atoms that are held by a weak magnetic field into an optical lattice by gradually turning on the optical potential to its desired strength. Upon increasing the intensity of the optical lattice to a critical intensity, the Bose-Einstein condensate (BEC) will undergo a quantum phase transition from a superfluid state to a Mott-insulator state [9]. One thereby can obtain one atom per lattice site in the ground state of the system; these atoms can serve as qubits. This suggestion of preparing a Mott-insulator state has recently led to a seminal experiment [12] wherein the quantum phase transition was observed. In principle, starting with a BEC in a trap and turning on an optical lattice of sufficient well depth in a sufficiently adiabatic manner, prepares the Mott-insulator state. In practice, it is easy to turn on the optical lattice adiabatically with respect to band excitation (excitation from one band to another); however, it is substantially more difficult to turn on the optical lattice adiabatically with respect to quasimomentum excitation. The second, more stringent form of adiabaticity requires that the optical lattice be switched on slowly with respect to mean-field interactions and tunneling dynamics between optical lattice sites, and hence typically requires milliseconds [10]. We refer to the first form of adiabaticity as "interband adiabaticity" and the second form as "intraband adiabaticity." The intraband adiabaticity condition has been demonstrated in one-dimensional lattices by Orzel *et al.* [11] and ultimately led to the pioneering experimental demonstration of the Mott-insulator transition [12].

The goal of this paper is to investigate the loading of atoms into an optical lattice in as short a time as possible, while maintaining interband adiabaticity, so as to obtain maximal atomic population in the ground state band with minimal band excitation. We consider experiments of the type described in Ref. [13], which measured the interband nonadiabaticity. We show how to optimize the turning on of a one-dimensional (1D) optical lattice so as to minimize the interband nonadiabaticity. We carry out calculations using the Gross-Pitaevskii (GP) equation, as well as simplified models. We show that an optimized lattice turn-on results in very low nonadiabaticity even for loading times t_r comparable to $1/\Delta\omega$, where $\hbar\Delta\omega$ is the excitation energy of the first band that can be excited. On such time scales, the nonlinear term in the GP equation is small and has little effect on the dynamics.

Section II discusses the theoretical models used, and describes how to determine the optimized turn-on of the lattice. It also describes a very simple unit cell model that is in excellent agreement with the full calculations. Section III describes our results and compares to experimental data. A final section summarizes our conclusions.

II. THEORY

Our theoretical investigation was stimulated by experimental work to load a BEC into a one-dimensional optical lattice so as to create the ground state of atoms in the optical lattice [13]. We first briefly describe the optical potential and its turn-on, then consider the mean-field description of the process, develop the simple unit-cell model, and finally describe the optimization procedure used.

A. The optical potential

We start with a condensate of N atoms in a trap with frequencies ν_x, ν_y, and ν_z. At time $t=0$, a 1D optical lattice with potential

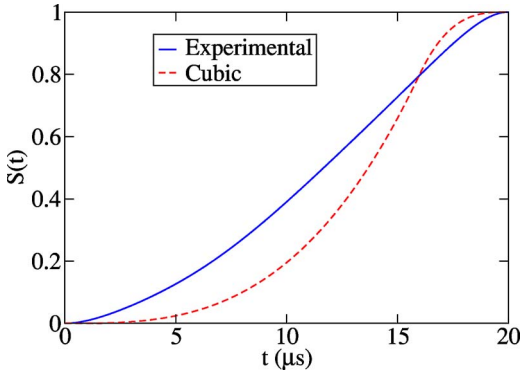

FIG. 1. (Color online) Fit to the experimental ramp function $S(t)$ used in Ref. [13], and piecewise cubic $S(t)$ with $t_r=20$ μs. In both functions $t_r=20$ μs.

$$V_L(x,t) = -S(t)V_0 \cos^2(kx) \tag{1}$$

is turned on along the x direction. The lattice periodicity equals π/k, where $k=\omega_L/c$ and $\omega_L/2\pi$ are the wave vector and frequency of the laser beams that form the optical lattice. The lattice beams are sufficiently far-detuned so that spontaneous emission is negligible on the time scale of the dynamics described here. The parameter V_0 is the final lattice depth after completion of the turn on process at ramp time t_r. The ramp turn-on function $S(t)$ has only two constrains, $S(0)=0$ and $S(t_r)=1$. For diagnostic purposes the lattice is held on with fixed depth V_0 until time $t_f=t_r+t_{\text{hold}}$, then turned off to allow for condensate expansion and imaging. Figure 1 shows two examples of ramp functions with $t_r=20$ μs, a piecewise cubic function with function and derivative matched at $t_m=16$ μs and a fit to the experimental ramp function used in Ref. [13].

B. Mean-field description

The GP equation for the BEC wave function $\Psi(\mathbf{r},t)$ (the order parameter of the condensate) is

$$i\hbar\frac{\partial\Psi}{\partial t} = -\frac{\hbar^2}{2m}\nabla^2\Psi + V(\mathbf{r},t)\Psi + \frac{4\pi\hbar^2 a}{m}|\Psi|^2\Psi, \tag{2}$$

where $V(\mathbf{r},t)=V_{\text{trap}}(\mathbf{r})$ for times $t<0$ and $V(\mathbf{r},t)=V_L(x,t)$ for $t\geqslant 0$, and the nonlinear term is proportional to the two-body s-wave scattering length a, and m is the atomic mass. We assume the trap is turned off at $t=0$. The lattice turn on time t_r is assumed to be very short compared to the time needed for the condensate to expand significantly.

The initial condensate wave function at $t=0$ is that for a trap with time-invariant potential $V_{\text{trap}}(\mathbf{r})$. Although the momentum distribution of the initial condensate wave function $\Psi(\mathbf{r},0)$ is sharply peaked close to zero, the final condensate wave function $\Psi(\mathbf{r},t_r)$ in the lattice has developed momentum components peaked near $0,\pm 2\hbar k,\pm 4\hbar k,\ldots$. These components appear even if only the ground state band of the lattice is occupied. Consequently, the subsequent free evolution of the condensate after t_f results in the further physical splitting of the condensate wave packet into spatially separate parts having central momenta $2n\hbar k$, where $n=0,\pm 1,\ldots$. The experiment consists of measuring the fraction $p_{nk}(t_f)$ of the initial total number of condensate atoms N that appear in the nth wave packet. As we describe below, the signature of nonadiabatic excitation during the turn-on of the ramp is oscillatory behavior of $p_{nk}(t_f)$ with varying hold times t_{hold}.

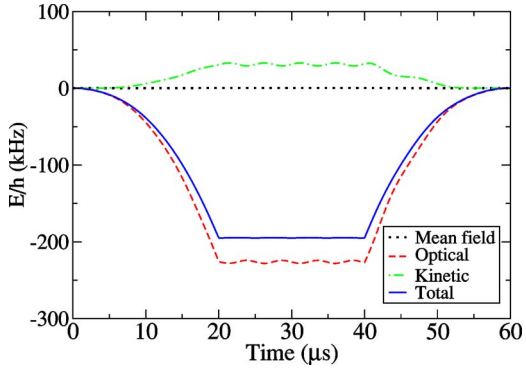

FIG. 2. (Color online) Kinetic, optical, mean-field and total energies versus time starting from a condensate with 10^4 Na atoms in a trap with frequencies of 84 Hz, 59.4 Hz, and 42 Hz in the respective x, y, and z directions. A 20 μs linear ramp is applied ending at a latttice depth of $V_0=14E_R$ followed by a 20 μs hold time and a 20 μs linear ramp down.

The central goal of this paper is to determine the optimized ramp function $S_{\text{opt}}(t)$ for a given t_r and V_0, i.e., the function $S(t)$ which leads to minimal oscillatory amplitude of $p_{nk}(t_f)$, and hence minimal excitation of the final condensate wave packet at time t_r [see Eq. (9)]. Our optimization will be carried out using the GP equation. We do not require that our system remain adiabatic during the whole time interval between $t=0$ and t_r, but only that the interband excitation be as small as possible at the final time t_r. It should be noted that the mean-field treatment used here cannot be used upon increasing the optical lattice potential to the point where the BEC undergoes a quantum phase transition from its BEC-like superfluid state to a Mott-insulator state. Once the number of atoms in each optical potential well becomes small (i.e., no longer large compared with unity), a field theory description must be used.

It is easy to calculate the experimental observables from the GP wave function $\Psi(x,t_f)$. By performing a Fourier transform it is easy to calculate the fraction $p_{nk}(t_f)$ of atoms associated with each sharply peaked momentum component n. The degree of interband nonadiabaticity f_{nonad} is determined experimentally by the amplitude of the oscillations in $p_{0k}(t_f)$ versus t_f,

$$f_{\text{nonad}} = p_{0k,\max} - p_{0k,\min}, \tag{3}$$

where $p_{0k,\max}$ and $p_{0k,\min}$ are the maximum and minimum values of $p_{nk}(t_f)$ for $n=0$ over an interval $t_f-t_r=t_{\text{hold}}$ which is chosen to be long enough to include at least one oscillation of $p_{0k}(t_f)$. If there is no interband excitation, then $f_{\text{nonad}}=0$.

Figure 2 shows various components of the BEC energy as they evolve in time when an optical potential with $2\pi/k=590$ nm, and $V_0=14E_R$, where the recoil energy E_R is defined as $E_R=\hbar^2k^2/2m$, is turned on linearly over 20 μs, held

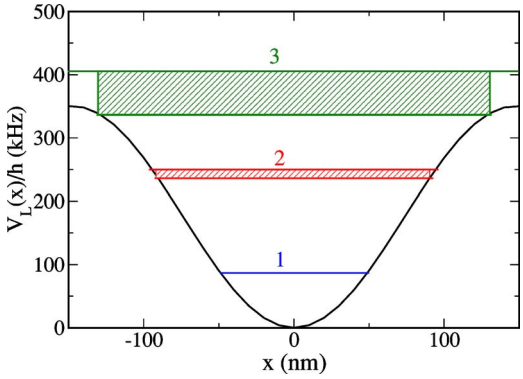

FIG. 3. (Color online) Unit cell lattice potential $V_L(x)$ versus x, showing the energy spread of the first three energy bands for a Na lattice with $2\pi/k=590$ nm and $V_0=14E_R$, where $E_R/h=25$ kHz.

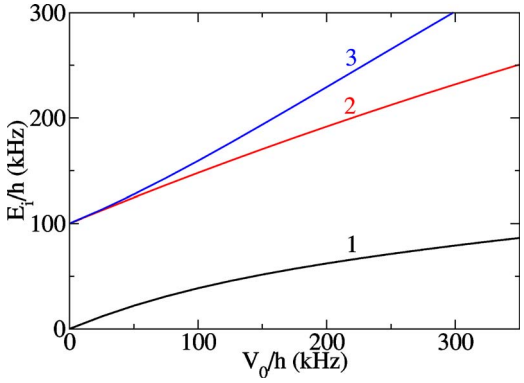

FIG. 4. (Color online) Energies of the first three $q=0$ levels versus lattice depth V_0/h for the unit cell shown in Fig. 2. The second and third levels are degenerate with an energy $4E_R$ in free space, but split into symmetric (E_3) and antisymmetric (E_2) states with increasing lattice depth. Turning on the lattice rapidly couples the symmetric $i=1$ ground and $i=3$ levels, but not the $i=2$ one.

constant for 20 μs, and finally turned off over 20 μs. The trap with frequencies $\nu_x=84$ Hz, $\nu_y=59.4$ Hz, and $\nu_z=42$ Hz holds 10^4 Na $F=1$, $M=-1$ atoms, for which $a=2.8$ nm and $E_R/h=25$ kHz. Notice that the total energy of the system is constant when the potentials do not depend on time. The mean field energy remains negligible in comparison to the kinetic and potential energies that result from turning on the optical potential. Consequently, calculations with 10 000 and 1×10^6 atoms are indistinguishable on the scale of Fig. 2. We also checked that on these short time scales the calculated nonadiabaticities from both 3D and 1D versions of the GP equations are indistinguishable. Thus, 1D linear Schrödinger dynamics should provide an excellent approximation to the nonadiabatic dynamics.

C. Unit-cell model

We only consider relatively short time scales t_r of lattice loading so that mean-field interactions do not play an important role, as shown in Sec. II B. We assume t_r is short compared with the nonlinear time $t_{\mathrm{NL}}\equiv m/(4\pi\hbar a|\Psi_{\mathrm{peak}}|^2)=\hbar/\mu$, where $|\Psi_{\mathrm{peak}}|^2$ is the peak value of $|\Psi|^2$ at $t=0$, and μ is the chemical potential. Consequently, we can develop a simple linear "unit cell" model of the loading process that is in excellent agreement with the full GP dynamics. In the unit cell model, the natural units of length, energy, and time are $1/k$, the recoil energy $E_R=\hbar^2k^2/2m$, and a characteristic lattice band excitation time $t_{\mathrm{band}}=2\pi/\Delta\omega$, respectively, where $\Delta\omega$ is the trap excitation parameter defined in the next paragraph.

Figure 3 shows the Wigner-Seitz primitive unit cell of an infinite optical lattice of depth $V_0=14E_R$. Solving the Schrödinger equation for the potential $-V_0\cos^2 kx$ with periodic boundary conditions on the interval $-\pi/2k\leqslant x\leqslant\pi/2k$ defines a series of eigenvalues $E_i(V_0)$ and eigenfunctions $|i,V_0\rangle$ that describe the unit cell wave function for the $q=0$ edge of each band i, where q is the lattice momentum [14]. The boxes in Fig. 3 indicate the width of the energy bands, obtained by calculating the energies of the Brillouin zone edges. The width of the lowest band is too narrow to be observed on the energy scale of the figure. The width of the third band extends beyond the top of the lattice potential. Figure 4 shows the energies E_i for the $q=0$ levels for the first three lattice bands as the lattice depth V_0 is increased. Since symmetry considerations only allow excitation of odd numbered bands from the first $n=1$ band during lattice turn on, the relevant trap excitation parameter $\Delta\omega$ is $(E_3-E_1)/\hbar$. For the example in Fig. 3, $\Delta\omega=2\pi(250\ \mathrm{kHz})$ and $t_{\mathrm{band}}=4$ μs.

An adiabatic basis set expansion can be used to calculate the time-dependent amplitudes $a_j(t)$ of the instantaneous eigenvectors during the dynamics. The basis set expansion is taken in the form

$$\Psi(t)=\sum_j a_j(t)e^{-i\int_0^t E_j(t')dt'/\hbar}|j(t)\rangle, \tag{4}$$

where $|j(t)\rangle$, $j=1,2,\ldots$, is the instantaneous eigenvector with energy eigenvalue $E_j(t)$ corresponding to an optical potential strength $S(t)V_0$. The nonadiabatic dynamics is then calculated from the coupled set of equations,

$$\dot{a}_i=\sum_{j\neq i}a_j(t)\frac{\langle i(t)|\dot{H}|j(t)\rangle}{E_i(t)-E_j(t)}e^{i[\alpha_j(t)-\alpha_i(t)]}.$$

where we have defined the coefficient $\alpha_j(t)=-\int_0^t E_j(t')dt'/\hbar$ to simplify the notation. The even index and odd index eigenstates are not coupled because the potential and its time derivative are an even function of x and the odd (even) eigenstates are symmetric (antisymmetric). We numerically calculate $E_i(t)$, $E_j(t)$, and $\langle i(t)|\dot{H}(t)|j(t)\rangle$, and solve the coupled differential equations by using a variable step size integrator. We will call this method the converged unit cell model.

We have verified by numerical calculations that a truncated basis set expansion with the lowest two terms is a good approximation unless the ramp time t_r becomes comparable to t_{band} or less,

$$\Psi(t)=a_1(t)e^{i\alpha_1(t)}|1(t)\rangle+a_3(t)e^{i\alpha_3(t)}|3(t)\rangle. \tag{5}$$

This leads to the following simplified two-equation unit cell model:

$$\dot{a}_1 = a_3(t)\frac{\langle 1(t)|\dot{H}|3(t)\rangle}{E_1(t) - E_3(t)}e^{i[\alpha_3(t)-\alpha_1(t)]}, \tag{6}$$

$$\dot{a}_3 = a_1(t)\frac{\langle 3(t)|\dot{H}|1(t)\rangle}{E_3(t) - E_1(t)}e^{i[\alpha_1(t)-\alpha_3(t)]}. \tag{7}$$

An even simpler one-equation approximation, which is acceptable for sufficiently large t_r, is to set $a_1=1+i0$ and solve for $a_3(t)$ by integrating Eq. (7), so that

$$a_3(t) = \int_0^t \frac{\langle 3(t')|\dot{H}|1(t')\rangle}{E_3(t') - E_1(t')}e^{i[\alpha_1(t')-\alpha_3(t')]}dt'. \tag{8}$$

We will call this the one-equation unit cell model.

The fraction of the total number of atoms in the wave packet with mean momentum nk, $p_{nk}(t)$, can be calculated in terms of the amplitudes $a_j(t)$,

$$\begin{aligned} p_{nk}(t) &= |\langle 2nk|\Psi(t)\rangle|^2 \\ &= \left|\sum_j a_j(t)\langle 2nk|j(t)\rangle e^{i\alpha_j(t)}\right|^2 \\ &\approx |a_1(t)\langle 2nk|1(t)\rangle e^{i\alpha_1(t)} + a_3(t)\langle 2nk|3(t)\rangle e^{i\alpha_3(t)}|^2. \end{aligned} \tag{9}$$

When $n>0$, the total population with magnitude of momentum $|nk|$ is

$$p_{|nk|}(t) = p_{nk}(t) + p_{-nk}(t). \tag{10}$$

The observable f_{nonad} in Eq. (3) can be calculated from $p_{0k}(t)$. Using the one-equation model of Eq. (8), where $a_1=1$, f_{nonad} simplifies to

$$f_{\text{nonad}} = 4\langle 0k|1\rangle\langle 0k|3\rangle|a_3|. \tag{11}$$

The expression in Eq. (11) is evaluated for $t>t_r$, where none of V_L, $|1\rangle$, $|3\rangle$, or $|a_3|$ is changing in time.

The fidelity F of the ramp can be defined as the fraction of population that is left in the ground state after the ramp, $F=|a_1|^2$, where $a_1(t)$ is evaluated for a time after t_r. In the two-state model, $F=1-|a_3|^2$. Using the result in Eq. (11), we can get a relation between F and f_{nonad},

$$F = 1 - \frac{1}{16|\langle 0k|1\rangle\langle 0k|3\rangle|^2}f_{\text{nonad}}^2. \tag{12}$$

For the case of the $V_0=14E_R$ Na lattice discussed in the figures, $F=1-0.28|f_{\text{nonad}}|^2$.

Figure 5 compares the numerical solutions for the two-equation model of Eqs. (6) and (7) and the one-equation model of Eq. (8) for a $V_0=14E_R$ lattice with the cubic ramp function in Fig. 1. Clearly, the simpler one-equation model provides a very good approximation in this case. Figure 5 shows that the degree of nonadiabaticity at the end of the ramp can be much smaller than during the turn-on portion of the ramp. This suggests that we might be able to optimize the ramp so that the final value of $|a_3|^2$ at the end of the ramp is small, even if it becomes large during the ramp.

Figure 6 shows the populations of the free space momentum states, $p_{0k}(t)$ and $p_{|2k|}(t)$, for several different calculations. The $V_0=14E_R$ lattice is turned on with the cubic ramp function in Fig. 1. Figure 6 shows the momentum state populations that correspond to the adiabatic eigenstates, $|\langle 2nk|j\rangle|^2$, as well as those obtained with dynamical calculations based on the GP equation and the two-equation unit cell model of Eqs. (6) and (7). Figure 6 demonstrates the very good agreement between the GP and unit cell model. The oscillations of the dynamical populations around the adiabatic ones are due to nonadiabatic excitation because of the fast ramp. The amplitude of these oscillations correspond to $f_{\text{nonad}}=0.07$ and a fidelity of $F=0.9985$.

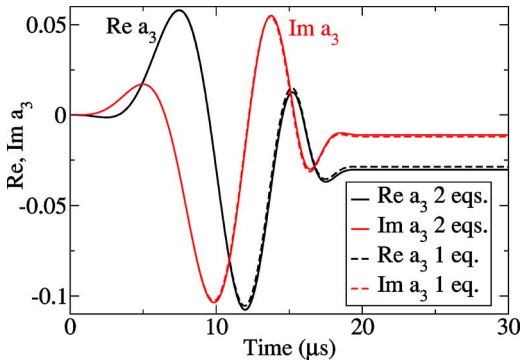

FIG. 5. (Color online) Time evolution of the real and imaginary parts of a_3 calculated with the $14E_R$ deep, 20 μs cubic ramp shown in Fig. 1. The results are shown for the two-equation model and the one-equation model. Equations (6), (7), and (8), respectively.

D. Optimization

The oscillations evident in Fig. 6 are due to the small but finite value of excitation at the final time t_f that reduces the fidelity F of the ramp. We will use an unconstrained nonlinear optimization to minimize the degree of nonadiabatic excitation at the end of the ramp and thus maximize the fidelity F. For this purpose we use an Nth order polynomial form for the ramp function $S(t)$, with $S(0)=0$ and $S(t_r)=1$. The form of $S(t)$ is given by

$$S(t) = \sum_{i=0}^{N+1} c_i t^i, \tag{13}$$

where $c_{N+1}=(1-\Sigma_{i=0}^{N} c_i t_r^i)/t_r^{N+1}$ insures that $S(t_r)=1$. We then can use a standard computer code that does unconstrained

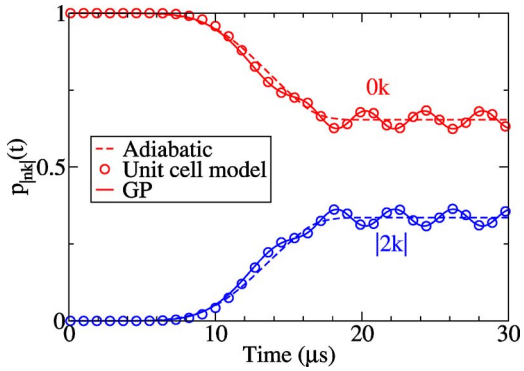

FIG. 6. (Color online) Population of the $0k$ and $|2k|$ momentum components versus time. The optical lattice is turned on to a depth of $14E_R$ with the 20 μs cubic ramp shown in Fig. 1.

nonlinear optimization to optimize the polynomial coefficients c_i, $i=1,\ldots,N$ to give the minimal f_{nonad}. We can minimize f_{nonad} calculated from the GP equation, or from the one-or two-equation unit cell models. We will use the GP equation, since this allows us to work with very short ramps, where the nonadiabaticity is large during the ramp. We will use the simpler models for interpreting the results. The polynomial form we have chosen for $S(t)$ is arbitrary. Any fitting function which meets the boundary conditions that $S(t)$ vanishes initially and goes to unity finally could be used, and the parameters in the function can be optimized so as to minimize f_{nonad}. We also note that different types of optimization algorithms, such as simulated annealing algorithms, could have been used instead of the algorithm we choose.

III. RESULTS

A. Comparison to experiment

In the experiment of Ref. [13], a BEC with 3×10^6 sodium atoms in the $3S_{1/2}$, $F=1$, $m_F=-1$ state with no discernible thermal component is prepared and held in a magnetic time-orbiting potential (TOP) trap with trapping frequencies in the x, y, and z directions of 27 Hz, 19 Hz, and 13.5 Hz. After production of the condensate, an optical lattice consisting of two counter-propagating laser beams along the x direction is turned on. The lattice beams are detuned about 60 GHz to the blue of the sodium $D2$ line at 589 nm. The spontaneous emission rate is negligible on the time scale of the experiments. The polarization is linear and parallel to the rotation axis of the TOP trap bias field (the y axis). The condensate is located in the focus of the beams, which have a $1/e^2$ beam diameter of about 600 μm.

In order to directly measure the adiabaticity, i.e., the efficiency of transfer into the lattice ground state, an experiment was carried out in which the intensity of the optical potential was ramped up to a stationary lattice potential strength $V_0 \approx 14E_R$ [13]. The BEC was held in the lattice for a time t_{hold}, typically between 0 and 10 μs, before suddenly switching off the light. The plane-wave decomposition of the lattice wave function at the switch-off time t depends on the previous history of the ramp prior to time t. The populations of the various momentum components at t is measured by allowing the atomic cloud to expand after the switch-off, since each $2nk$ momentum component eventually separates from the others in an individual cloud that can be imaged. Figure 7 shows calculated and observed oscillations for the population of the $0k$ component following a ramp of 20 μs. This beating signal has a small amplitude, indicating that most of the population was in the lowest band. However, if only the ground state were populated, there would have been no beating at all.

Figure 7 also shows our calculation of $p_{0k}(t)$ using the GP equation with the experimental lattice potential having the ramp shown in Fig. 1. The figure shows the original data of Ref. [13] as well as data that has been shifted in phase and magnitude to coincide with the calculation. These adjustments are consistent with an experimental uncertainty in the lattice depth V_0 of about 10% and the uncertainty in the ramp function. Even without the adjustments, it is clear that our calculation gives the right magnitude of the effect of nonadiabatic dynamics as measured by the oscillations in the signal after t_r.

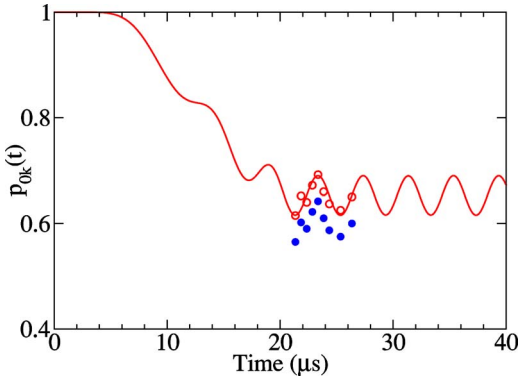

FIG. 7. (Color online) Comparison of theory and NIST experimental data (closed circles) [13] on the population of the $0k$ momentum component versus time for the experimental 20 μs ramp shown in Fig. 2 for a $V_0=14E_R$ deep optical lattice. The open circles shows data shifted to have the same peak magnitude as that of the calculation.

B. Ramp optimization results

Although the degree of nonadiabaticity in Fig. 7 is small, it can be made even smaller by optimizing the ramp turn-on function. We used a numerical optimization algorithm to minimize f_{nonad} as defined in Eq. (3) versus the polynomial fit parameters in Eq. (13). We calculated the dynamics with the GP equation, the one-equation unit cell model, the two-equation unit cell model, and the converged unit cell model. The one-equation unit cell model works very well except for short ramps with t_r on the order of t_{band}. Only the GP and the converged unit cell model work well in this limit, due to excitation of higher bands that are not modeled within the one-or two-equation unit cell model.

Figure 8 shows the optimal ramps obtained for several different ramp durations, $t_r=6$, 10, 15, and 20 μs, using ramp polynomial functions of order $N=6$ and $N=12$ in Eq.

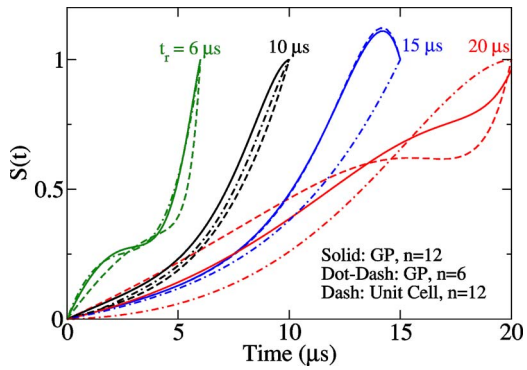

FIG. 8. (Color online) Optimal ramp functions for 6, 10, 15, and 20 μs ramps for a $14E_R$ lattice. The solid and dotted-dashed curves were calculated in the GP equation and $N=12$ and 6, respectively, while the dashed curves were calculated with the two-equation unit cell model with $N=12$.

TABLE I. Nonadiabaticities f_{nonad} associated with the optimal curves shown in Fig. 8.

t_r	$N=6$	$N=12$
6 μs	4.42×10^{-3}	2.50×10^{-3}
10 μs	1.10×10^{-3}	4.92×10^{-4}
15 μs	9.62×10^{-4}	9.89×10^{-4}
20 μs	9.73×10^{-5}	1.75×10^{-4}

(13), starting the optimization with a linear ramp function. Clearly, the optimal ramp shape depends strongly on the ramp duration. All the fidelities obtained using optimized ramps were very close to unity for all ramp durations (much closer to unity than those obtained without optimization). In order to show the sensitivity to the order of the polynomial function used, we plot the optimal ramps obtained with the GP equation for $N=6$ and $N=12$ ramps as dotted-dashed and solid curves, respectively, as indicated in Table I which tabulates f_{nonad} for all the GP results shown in Fig. 8. The fidelity is calculated from f_{nonad} using Eq. (12). Although the fidelities obtained are very close to unity for both values of N (and all t_r), the resulting optimized ramps for a given t_r can vary with N. There are often many minima in parameter space with fidelities that are very close to unity, and the optimization routine we used can get stuck in a local minimum.

Figure 8 also shows optimized ramps obtained using the two-equation unit cell model with $N=12$. The unit cell calculation can result in the optimization routine finding a different local minimum than the one found using the GP equation (see the $t_r=20$ μs curves). Moreover, different optimal ramps can be obtained upon starting with varying initial functions for $S(t)$, e.g., a cubic rather than a linear initial ramp function. To summarize, the optimization functional being minimized can have several local minima so that several different optimized functions can have similar high fidelities.

Figure 9 shows $a_3(t)$ versus time for the optimal 6 μs and 20 μs ramps in Fig. 8. In both cases, there is clearly significant excitation during the ramp, however, at the end of the ramps, the excitation is nearly zero. Hence, the dynamics is clearly nonadiabatic for both ramps, but at the final time t_r, there is very little excitation, i.e., high fidelity is achieved for both ramps. With the optimized ramps, the fidelity obtained is much higher than that obtained in the NIST experiment, even with the 6 μs ramp. However, the a_3 coefficients in Fig. 9 go to zero at the end of the ramps with a high slope, suggesting that the fidelity might not be robust with respect to small changes in the ramp parameters. Also, for small t_r, the optimized ramp functions can vary dramatically and suddenly with time and therefore may be difficult to achieve experimentally.

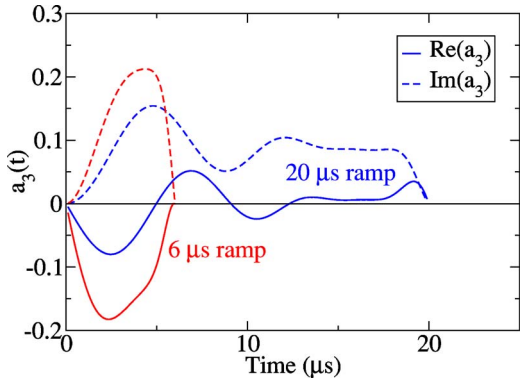

FIG. 9. (Color online) Real and imaginary parts of the amplitude $a_3(t)$ versus time for 6 and 20 μs optimal ramps, showing strong nonadiabatic behavior as a function of time, but ending at t_r with very small excitation.

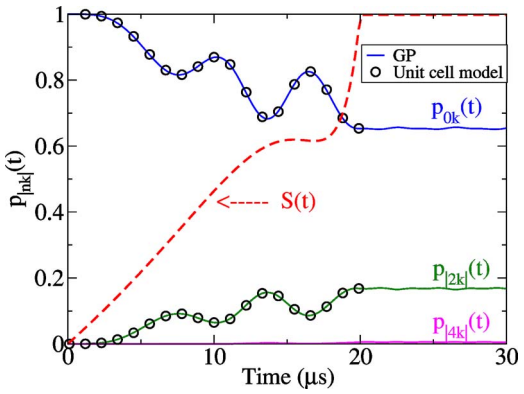

FIG. 10. (Color online) GP and unit cell populations versus time for optimal 20 μs ramp. The fidelity is 0.999 999.

Figures 10 and 11 show the calculated $0k$ and $|2k|$ populations versus time as determined using the full GP equation and the converged unit cell model for the optimal 20 and 6 μs ramps, respectively. The $S(t)$ ramp functions are also shown in the figures. The converged unit cell model reproduces the GP results very accurately, even for the 6 μs ramp. For the 6 μs ramp, there is already a small $4k$ population component present. Nevertheless, the fidelity remains high.

IV. SUMMARY

We calculated the dynamics of a BEC upon turning on a one-dimensional optical potential. Good agreement with ex-

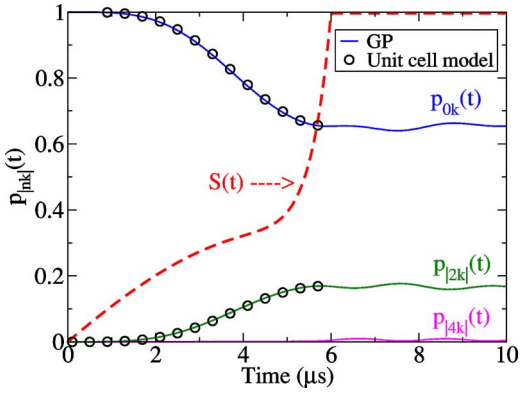

FIG. 11. (Color online) GP and unit cell populations versus time for optimal 6 μs ramp. The fidelity is 0.9996.

perimental data has been obtained. We showed that the optimal ramp function $S(t)$, with $S(0)=0$ and $S(t_r)=1$, for turning on a one-dimensional optical lattice potential, $V_L(x,t)=S(t)V_0\cos^2(kx)$, can be chosen to minimize the interband nonadiabaticity. A simple unit cell model that is in excellent agreement with the full calculations has been developed for cases when the turn-on time t_r is relatively long. An optimized lattice turn-on with very low nonadiabaticity can be chosen even for short loading times t_r comparable to $2\pi/\Delta\omega$, where $\hbar\Delta\omega$ is the band excitation energy.

Even if the loading of a BEC into the lattice without causing interband excitation is readily achievable, as shown here, unless one switches on an optical lattice very slowly, the optical lattice causes a spatially varying phase to accumulate across the condensate due to intraband excitation. Reference [10] has shown analytically and numerically that a cancellation of this effect is possible by appropriately adjusting the harmonic trap force constant of the external magnetic trap that confines that BEC, thereby facilitating quick loading of an optical lattice for quantum computing purposes.

ACKNOWLEDGMENTS

This work was supported in part by grants from the Office of Naval Research, the U.S.-Israel Binational Science Foundation (Grant No. 2002147), the Israel Science Foundation for a Center of Excellence (Grant No. 8006/03), and the German Federal Ministry of Education and Research (BMBF) through the DIP project. M.T. was supported by the Polish Ministry of Scientific Research and Information Technology under grant PPZ MIN-008/P03/2003.

[1] J. I. Cirac and P. Zoller, Phys. Rev. Lett. **74**, 4091 (1995).
[2] M. Brune, P. Nussenzveig, F. Schmidt-Kaler, F. Bernardot, A. Maali, J. M. Raimond, and S. Haroche, Phys. Rev. Lett. **72**, 3339 (1994).
[3] Q. A. Turchette, C. J. Hood, W. Lange, H. Mabuchi, and H. J. Kimble, Phys. Rev. Lett. **75**, 4710 (1995).
[4] N. A. Gershenfeld and I. L. Chuang, Science **275**, 350 (1997).
[5] D. P. DiVincenzo, J. Magn. Magn. Mater. **200**, 202 (1999).
[6] Y. Nakamura, Yu. A. Pashkin, and J. S. Tsai, Nature (London) **398**, 786 (1999); J. E. Mooij *et al.*, Science **285**, 1036 (1999); L. B. Ioffe *et al.*, Nature (London) **398**, 679 (1999).
[7] G. K. Brennen, C. M. Caves, P. S. Jessen, and I. H. Deutsch, Phys. Rev. Lett. **82**, 1060 (1999).
[8] D. Jaksch, H.-J. Briegel, J. I. Cirac, C. W. Gardiner, and P. Zoller, Phys. Rev. Lett. **82**, 1975 (1999).
[9] D. Jaksch, C. Bruder, J. I. Cirac, C. W. Gardiner, and P. Zoller, Phys. Rev. Lett. **81**, 3108 (1998).
[10] S. E. Sklarz, I. Friedler, and D. J. Tannor, Y. B. Band, and C. J. Williams, Phys. Rev. A **66**, 053620 (2002).
[11] C. Orzel, A. K. Tuchman, M. L. Fenselau, M. Yasuda, and M. A. Kasevich, Science **291**, 2386 (2001).
[12] M. Greiner, O. Mandel, T. Esslinger, T. W. Hänsch, and I. Bloch, Nature (London) **415**, 39 (2002).
[13] J. Hecker Denschlag, J. E. Simsarian, H. Häffner, C. McKenzie, A. Browaeys, D. Cho, K. Helmerson, S. L. Rolston, and W. D. Phillips, J. Phys. B **35**, 3095 (2002).
[14] Although we used a numerical solution for the potential, the analytic solution to the Mathieu equation could also be used.